

# Non-Abelian plasma instabilities: SU(3) vs. SU(2)

Andreas Ipp and Anton Rebhan

*Institut für Theoretische Physik, Technische Universität Wien,  
Wiedner Hauptstraße 8-10, A-1040 Vienna, Austria*

Michael Strickland

*Department of Physics, Gettysburg College, Gettysburg, PA 17325, USA*

We present the first 3+1 dimensional simulations of non-Abelian plasma instabilities in gauge-covariant Boltzmann-Vlasov equations for the QCD gauge group SU(3) as well as for SU(4) and SU(5). The real-time evolution of instabilities for a plasma with stationary momentum-space anisotropy is studied using a hard-loop effective theory that is discretized in the velocities of hard particles. We find that the numerically less expensive calculations using the group SU(2) essentially reproduce the nonperturbative dynamics of non-Abelian plasma instabilities with higher rank gauge groups provided the mass parameters of the corresponding hard-loop effective theories are the same. In particular we find very similar spectra for the turbulent cascade that forms in the strong-field regime, which is associated with an approximately linear growth of energy in collective fields. The magnitude of the linear growth however turns out to increase with the number of colors.

PACS numbers: 11.15.Bt, 04.25.Nx, 11.10.Wx, 12.38.Mh

## I. INTRODUCTION

Non-Abelian plasma instabilities are, parametrically, the dominant collective phenomenon in a weakly coupled quark-gluon plasma, and have been discussed as a possible explanation for the extremely fast isotropization that is suggested by the success of hydrodynamical models of relativistic heavy-ion collisions [1]. Such plasma instabilities are generalizations of the so-called Weibel or filamentary instabilities in ordinary electromagnetic plasmas [2]. They are present already in collisionless plasmas with any amount of momentum space anisotropy [3, 4], and, indeed, they have been found to play an important role in the fast isotropization of electromagnetic plasmas [5]. Their non-Abelian versions have been proposed to be of relevance for the quark-gluon plasma early on by Mrówczyński and others [6–15], and specifically as explanation for the fast apparent thermalization by Arnold et al. [16, 17].

Numerically, these instabilities have been studied in a discretized version of the hard-loop approximation [18–20], which corresponds to gauge covariant Boltzmann-Vlasov equations describing the dynamics of (soft) collective fields in a weakly coupled plasma of hard particles. The growth rate of plasma instabilities is parametrically of the same order as plasma frequencies and screening masses, and because of their exponential behavior the plasma instabilities dominate the collective dynamics and inevitably lead to nonperturbatively large collective fields. Eventually they will give rise to substantial backreactions on the momentum distribution of the hard particles, causing a breakdown of the hard-loop approximation [21–23] coincident with the actual isotropization process. The hard-loop approximation allows to study the early stage of this assumed scenario and thus its basis.

In the earliest stages of heavy-ion collisions it is in

fact important to take into account the expansion of the plasma, which modifies the growth from exponential in time to exponential in the square root of (proper) time, as indeed found in numerical simulations within the color glass condensate scheme [24, 25] as well as in a generalization of discretized hard loop simulations [26, 27]. In those simulations, an uncomfortable delay of the onset of growth has been observed, which however has recently been shown to largely disappear upon consideration of more general initial conditions [28]. While the density and lifetime of the plasma estimated for heavy-ion collisions at RHIC may be too low to give an important role to nonabelian plasma instabilities there, the higher values expected for LHC heavy-ion collisions may be sufficient for nonabelian plasma instabilities to become the dominant phenomenon in a less strongly coupled environment.

By means of real-time lattice simulations for stationary anisotropic plasmas, it has however been found that in contrast to effectively 1+1 dimensional situations where only the most unstable modes are considered, the exponential growth of non-Abelian plasma instabilities is limited in 3+1 dimensions by non-Abelian self-interactions. At a certain magnitude of the nonabelian fields, which depends on the degree of anisotropy [29, 30], the exponential growth ceases and turns into a linear growth of the energy densities of the soft fields. In that regime, a turbulent cascade of energy is observed, with a quasi-steady-state power-law distribution  $f_k \propto k^{-\nu}$  and spectral index  $\nu \approx 2$ , which transports the energy fed into low-lying modes by Weibel instabilities to stable higher-momentum (plasmon) modes through non-Abelian self-interactions of gluon fields [31]. This cascade forms at momentum scales that are parametrically separated from those of the hard particles, making it possible to study this phenomenon self-consistently within the hard-loop approximation. On the other hand, classical-statistical

simulations in SU(2) gauge theory [32, 33], where there is no such separation of scales, have reported a late-time behavior indicative of a lower index of  $\nu = 4/3$  (as in turbulence with constant transport of particle number) while showing an early behavior qualitatively similar to those of Chromo-Weibel plasma instabilities. The index  $\nu = 2$  found in the hard-loop simulations was argued [34] to fit to an energy cascade carried by particles in the cascade scattering off of nonperturbatively large background fields. However, this is not consistent with a steady-state particle cascade [35] (particle number of cascade particles is unchanged in the assumed process) so that either other processes are equally important or the resulting cascade is not steady-state. (See also Refs. [22, 23, 36–42] for discussions of instabilities and turbulence in QCD.)

In this paper we confirm the results [19, 20, 29–31] obtained for stationary anisotropic plasmas in the hard-loop framework for gauge group SU(2), and consider, for the first time, 3+1-dimensional hard-loop simulations for the QCD gauge group SU(3), as well as for SU(4) and SU(5), in order to quantify the dependence on the number of colors. So far, in the hard-loop effective theory, SU(3) calculations have only been performed for effectively 1+1 dimensional situations [20]. (In classical-statistical 3+1-dimensional lattice gauge theory the gauge group SU(3) has been studied in Ref. [43].)

## II. SETUP

In order to study nonabelian plasma instabilities in a weakly coupled quark-gluon plasma, which may for the first time become physically relevant at the higher temperatures and densities reached in heavy-ion collisions at the LHC, we consider the extreme limit of an ultrarelativistic collisionless plasma, where the main dynamics takes place at scales parametrically soft compared to the hard scale  $|\mathbf{p}| = p^0$  of the plasma constituents. In an isotropic plasma, the scale  $g|\mathbf{p}|$ , where  $g$  is the gauge coupling, determines the scale of the Debye screening mass, of the plasma frequency, and of Landau damping, but in an anisotropic plasma, the dominant collective phenomenon at this scale, which is larger than the scale of collisions, turns out to be plasma instabilities.

The effective field theory relevant for the collective phenomena at this largest of the soft scales is given by gauge-covariant collisionless Boltzmann-Vlasov equations [44] or “hard-loop” effective theory as long as the soft gauge fields obey  $A_\mu \ll |\mathbf{p}|/g$  so that a backreaction on the hard particles can still be ignored. This allows one to study in detail the first stage of plasma instabilities, which, as briefly reviewed in the introduction, is highly nontrivial in nonabelian gauge theories.

The corresponding effective action, which is nonlocal and nonlinear [45, 46], can be made local at the expense of introducing auxiliary fields [47] in the adjoint representation,  $W_\beta(x; \mathbf{v})$ , for each spatial unit vector appearing in the velocity  $v^\mu = p^\mu/|\mathbf{p}| = (1, \mathbf{v})$  of a hard (ultra-

relativistic) particle with momentum  $p^\mu$ . The  $W$  fields encode the fluctuations of the distribution function of colored hard particles. In terms of these, the induced current  $j$  in the nonabelian Maxwell equations

$$D_\mu(A)F^{\mu\nu} = j^\nu, \quad (1)$$

is given by

$$j^\mu[A] = -g^2 \int \frac{d^3\mathbf{p}}{(2\pi)^3} \frac{1}{2|\mathbf{p}|} p^\mu \frac{\partial f(\mathbf{p})}{\partial p^\beta} W^\beta(x; \mathbf{v}), \quad (2)$$

and the nonabelian Boltzmann-Vlasov equation, in which the scale of the ultrarelativistic hard particles drops out, reduces to

$$[v \cdot D(A)]W_\beta(x; \mathbf{v}) = F_{\beta\gamma}(A)v^\gamma, \quad (3)$$

with  $D_\mu = \partial_\mu - ig[A_\mu, \cdot]$ . (Our metric convention is  $(+ - - -)$ .)

We shall only consider a background distribution function  $f(\mathbf{p})$  of hard particles with one direction of anisotropy, obtained by deforming an isotropic distribution according to

$$f(\mathbf{p}) \propto f_{\text{iso}}(\mathbf{p}^2 + \xi p_z^2) \quad (4)$$

which leads to

$$\begin{aligned} j^\mu(x) &= \int \frac{d\Omega_{\mathbf{v}}}{4\pi} [a(\mathbf{v})W^0(x; \mathbf{v}) + b(\mathbf{v})W^z(x; \mathbf{v})] v^\mu \\ &\equiv \int \frac{d\Omega_{\mathbf{v}}}{4\pi} \mathcal{W}(x; \mathbf{v}) v^\mu, \end{aligned} \quad (5)$$

and

$$a(\mathbf{v}) = \frac{m^2}{(1 + \xi v_z^2)}, \quad b(\mathbf{v}) = \xi v_z a(\mathbf{v}), \quad (6)$$

with the mass parameter  $m$  proportional to  $g$  and the scale of the momenta of hard particles.

In the numerical treatment we discretize the 3-dimensional configuration space by cubic lattices, and the unit sphere by a set of unit vectors  $\mathbf{v}$  pointing to

$$\begin{aligned} z_i &= -1 + (2i - 1)/N_z, \quad i = 1 \dots N_z, \\ \varphi_j &= 2\pi j/N_\varphi, \quad j = 1 \dots N_\varphi \end{aligned} \quad (7)$$

in cylindrical coordinates. At each lattice site we thus introduce  $\mathcal{N}_{\mathcal{W}} = \mathcal{N}_z \times \mathcal{N}_\varphi$  variables  $\mathcal{W}_{\mathbf{v}}(x)$  whose dynamics is approximated by [18, 20]

$$\begin{aligned} [v \cdot D(A)]\mathcal{W}_{\mathbf{v}} &= (a_{\mathbf{v}}F^{0\mu} + b_{\mathbf{v}}F^{z\mu})v_\mu \quad (8) \\ D_\mu(A)F^{\mu\nu} &= j^\nu = \frac{1}{\mathcal{N}} \sum_{\mathbf{v}} v^\nu \mathcal{W}_{\mathbf{v}}. \quad (9) \end{aligned}$$

A different possibility of discretization was used in Ref. [19], where the auxiliary fields  $W^\mu(x; \mathbf{v})$  are expanded in spherical harmonics  $Y_{lm}(\mathbf{v})$  and truncated at some  $l_{max}$ .

In the following we shall consider a momentum space distribution of hard modes which is oblate, by choosing  $\xi = 10$  as before in Refs. [18, 20]. In this situation, a prolate region in momentum space at soft scales, pinched at the origin and involving longitudinal momentum  $0 < |k_z| < \mu = 1.072m$ , contains unstable modes. The mode with largest growth rate  $\gamma_* = 0.12m$  is found at  $\mathbf{k}_\perp = 0$  and  $k_z = k_* = 0.398m$ . The mass parameter  $m$  defined above is related to the asymptotic mass of propagating transverse gluons by  $m_\infty = 0.447m$ .

The details of the lattice discretization of the above nonabelian gauge-covariant Boltzmann-Vlasov equations can be found in the appendix of Ref. [20]. The only place where those formulae need to be modified to allow for general  $N_c$  is in the expression for the energy density. For arbitrary  $N_c$ , the chromo-magnetic part of the energy density in Eq. (B18) of Ref. [20] reads

$$\mathcal{E}_B = \frac{2N_c}{g^2 a^4} \sum_{\square} \left( 1 - \frac{1}{N_c} \text{tr} U_{\square}(t, x) \right). \quad (10)$$

In the numerical simulations of the above equations we have used parallelization on computer clusters, splitting up the simulation domain so as to fit into the main memories of the individual nodes, and considered total spatial lattices ranging from  $32^3$  to  $128^3$  and numbers of  $\mathcal{W}$  fields  $\mathcal{N}_{\mathcal{W}} = \mathcal{N}_z \times \mathcal{N}_\varphi = 20 \times 16 = 320$  and higher at each site, in addition to the  $N_g = N_c^2 - 1$  gluon fields (link variables) and their conjugate momenta.

The physical size of the lattice is determined by the parameter  $m^2$  appearing as prefactor in the induced current, Eq. (5). In terms of the asymptotic thermal mass of gluons, the lattice spacings that we have considered vary from  $am_\infty = 0.5656$  to  $0.1414$ . For the specific anisotropy that we are considering, this corresponds to  $a/(\lambda_*/2) = 0.16 \dots 0.04$  in terms of the wave length of maximal growth  $\lambda_*$ , or, with respect to the minimal wave length  $\lambda_\mu$  for which unstable modes exist:  $a/(\lambda_\mu/2) = 0.432 \dots 0.108$ .

In order to provide seed fields, we have initialized with vanishing gauge fields and

$$\langle \mathcal{W}_\mathbf{v}^a(0, x) \mathcal{W}_\mathbf{v}^b(0, y) \rangle = \delta^{ab} \delta_{x,y}^3 \sigma^2 a^3, \quad (11)$$

where  $\delta_{x,y}^3$  denotes 3 Kronecker deltas, subtracting  $\sum_{\mathbf{v}} \mathcal{W}^a / \mathcal{N}_{\mathcal{W}}^2$  from each  $\mathcal{W}^a$  in order to obey Gauss's law.

### III. NUMERICAL RESULTS

#### A. Growth of energy densities in chromo-electromagnetic fields

In the following we shall concentrate on the case of small initial fields (small  $\sigma$ ) so that there is first a phase of essentially Abelian evolution with exponential growth due to the Weibel instability, which ends when the gauge

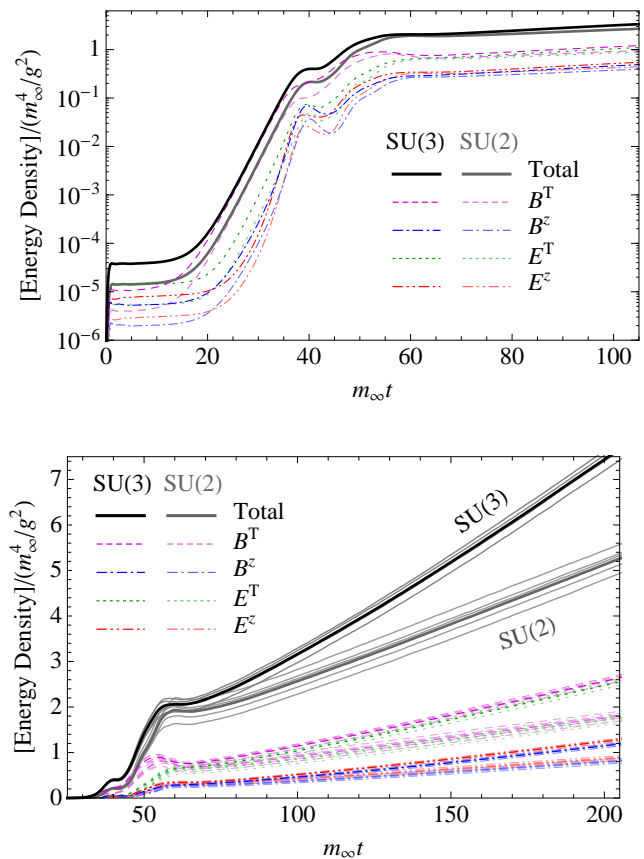


FIG. 1: (Color online.) Comparison of average energy densities  $\mathcal{E}$  for SU(2) (light) and SU(3) (dark) on logarithmic (upper panel) and linear (lower panel) scale in 3+1 dimensional simulations for anisotropy parameter  $\xi = 10$  on a  $64^3$  lattice with  $am_\infty = 0.5656$  (i.e.,  $a = 0.16(\lambda_*/2)$ ,  $L = 64a = 13.8\lambda_\mu$ ) and  $\mathcal{N}_{\mathcal{W}} = 320$  ( $= \mathcal{N}_z \times \mathcal{N}_\varphi = 20 \times 16$ ). The initialization of the  $\mathcal{W}$  fields is chosen with parameter  $\sigma = 0.1$  resulting in equal initial field amplitudes per gluon degree of freedom for both gauge groups. Shown are the total field energy densities as well as the contributions from transverse and longitudinal chromo-electric and chromo-magnetic fields. In the lower panel, the individual runs are shown by light curves.

fields have grown to nonperturbatively large amplitudes so that non-Abelian self interactions become important. We keep fixed the anisotropy parameter  $\xi = 10$  in all of the following comparisons.

For initially small fields, Figure 1 shows a comparison between SU(2) and SU(3) simulations. The simulations have been initialized with random fluctuations in the  $\mathcal{W}$  field with strength  $\sigma = 0.1$  for both gauge groups. Depicted is the total energy density and its contributions from chromo-electric and chromo-magnetic fields, each decomposed into parts transverse and longitudinal with respect to the direction of anisotropy. The SU(2) result has been obtained from averaging over 6 runs with different initial conditions, while for SU(3) 3 runs have been

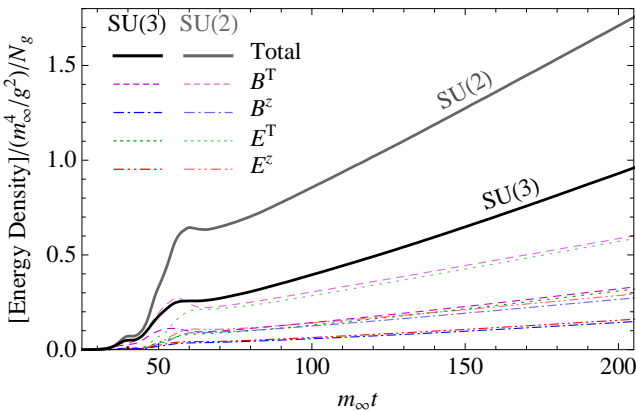
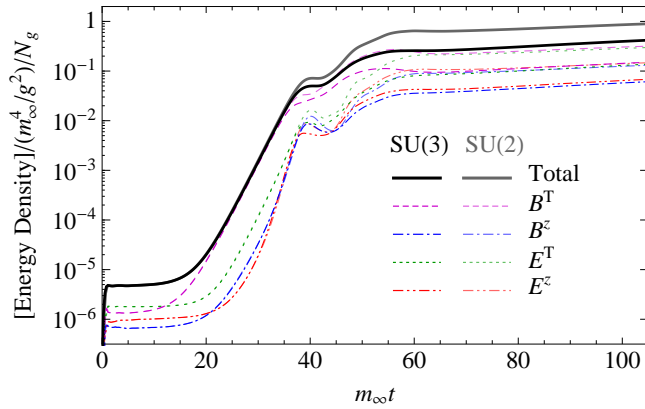


FIG. 2: (Color online.) Same as Fig. 1 for the energy density divided by the number of gluons  $N_g$ .

used. Because there are 8 gluons in SU(3) compared to 3 gluons in SU(2) that are initialized with the same average gauge field amplitude, the initial total energy density of SU(3) is larger than the SU(2) energy density by a factor  $8/3$ . Remarkably, at the end of the exponentially growing phase around  $m_\infty t \sim 60$  when the approximately linear growth regime sets in, the total energy densities approximately agree (after averaging over individual runs—the saturation energy of individual runs varies substantially, in particular for smaller lattice size). We have checked in comparison runs restricted to an Abelian U(1) subgroup that this agreement is not caused by the lattice spacing chosen and that we are safely below the compactness bound. The plot in linear scale shows that the SU(3) result subsequently grows somewhat faster than the SU(2) result.

In Fig. 2 the same results are compared by dividing by the number of gluons  $N_g$ . Now the SU(2) and SU(3) curves agree in the exponentially growing phase, with the SU(3) result starting to lag behind the SU(2) result from  $m_\infty t \sim 35$  onwards. In the linear growth regime, it is now the SU(2) curve that grows faster. Therefore the dependence of the linear growth rate in the non-Abelian

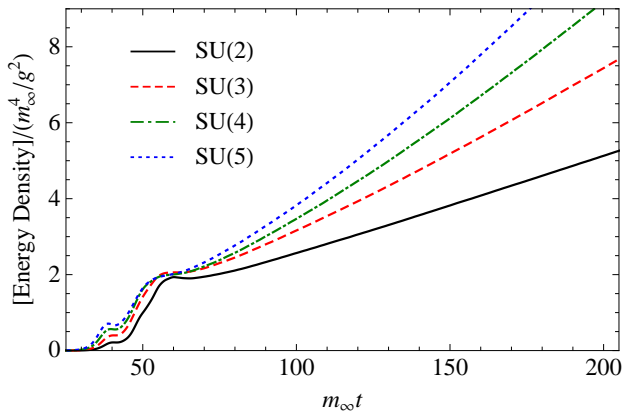
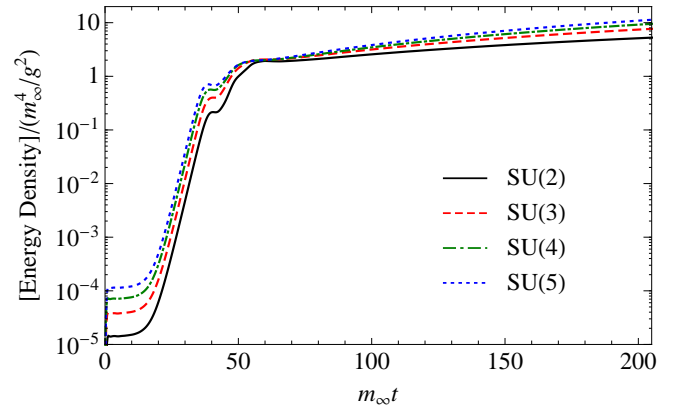


FIG. 3: (Color online.) Comparison of average total field energy densities  $\mathcal{E}$  for SU(2) through SU(5) on logarithmic (upper panel) and linear (lower panel) scale in 3+1 dimensional simulations for anisotropy parameter  $\xi = 10$  on a  $64^3$  lattice with  $\mathcal{N}_W = 320$  ( $= N_Z \times N_\phi = 20 \times 16$ ). The initialization of the  $\mathcal{W}$  fields is chosen with parameter  $\sigma_{\text{SU}(2)} = \sigma_{\text{SU}(3)} = \sigma_{\text{SU}(4)} = \sigma_{\text{SU}(5)} = 0.1$ .

regime on  $N_c$  seems to be a factor between 1 and  $N_g$ .

In order to study the systematics of the scaling with  $N_c$  in the non-Abelian regime, we extend the gauge group SU( $N_c$ ) to larger values of  $N_c$ . Figure 3 shows a comparison for gauge groups SU(2) through SU(5). This confirms the observation of Fig. 1 that the energy densities stop to grow at approximately the same value for different gauge groups, and also that the energy densities of the larger gauge groups grow faster in the regime of linear growth.

In Fig. 4 we plot the ratio of the time derivatives of the energy densities of Fig. 3 for the various gauge groups, all with same lattice parameters and initial gauge field strengths. Since the discrete derivatives wiggle strongly, the energy densities have been smoothed by averaging over a rectangular window function of size  $m_\infty \Delta t = 2$ . These results indicate that the slope of the energy density in the linear growth regime scales approximately proportional to the number of colors,  $N_c$ .

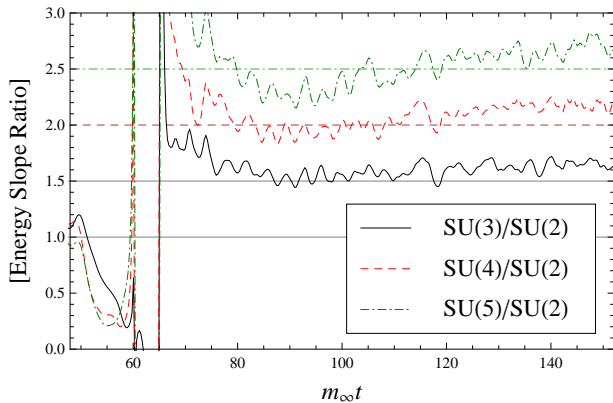


FIG. 4: (Color online.) The ratio of the time derivative of the energy densities of Fig. 3 for gauge groups SU(3), SU(4), and SU(5), divided by the one of SU(2). For large times, this is seen to scale approximately with  $N_c$ . Horizontal lines at  $3/2$ ,  $4/2$ , and  $5/2$  mark the ratios for scaling by the number of colors.

In Fig. 5 we show the slope ratio of gauge groups SU(3) and SU(2) for finer lattices (higher ultraviolet cutoff) at equal (but now smaller) physical volume size. For these curves, a rectangular window function of size  $m_\infty \Delta t = 10$  has been used. The data summarize averages over (a) 20, (b) 8, (c) 3 runs with different random initial conditions for SU(2), (a) 3, (b) 4, (c) 1 runs for SU(3), and one run for SU(5). In these runs, which have less resolution in the infrared, we still find ratios that are consistently larger than 1, but more scattered about the ratio of the number of colors. A scaling by number of colors is also supported by the slope ratio of SU(5) and SU(2) in Fig. 5. We are therefore led to the conjecture that the linear growth rate in the non-Abelian regime is proportional to  $N_c$ , but have to concede that our numerical verification involves sizeable uncertainties.

## B. Spectra

In order to get a glimpse of the underlying dynamics, following Ref. [31] we consider distribution functions of modes

$$\begin{aligned} f_A(k) &= \frac{k}{N_{\text{dof}}V} \langle \mathbf{A}^2(k) \rangle, \\ f_E(k) &= \frac{1}{N_{\text{dof}}kV} \langle \mathbf{E}^2(k) \rangle, \end{aligned} \quad (12)$$

where  $V$  is the total spatial volume and  $N_{\text{dof}} = 2N_g$  accounts for two transverse polarization states and  $N_g = N_c^2 - 1$  adjoint color states of the SU( $N_c$ ) gauge theory. The spectra are obtained from a Fourier transformation of the  $\mathbf{A}$  and  $\mathbf{E}$  fields in the lattice Coulomb gauge [48], which fixes the residual gauge freedom of the temporal

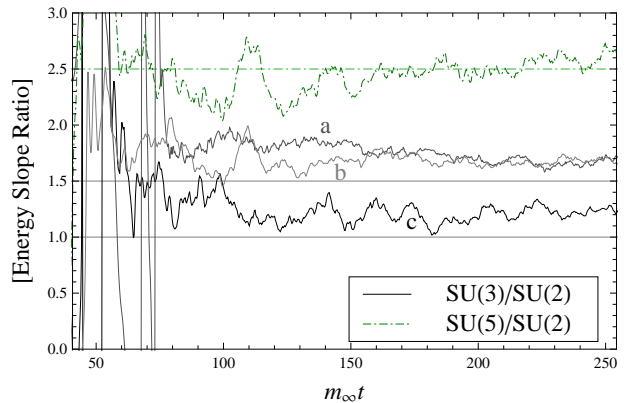


FIG. 5: (Color online.) The ratio of the time derivative of the energy densities for various lattice parameters. (a)  $32^3$ ,  $am_\infty = 0.2828$ ,  $\sigma = 0.0707$ ; (b)  $32^3$ ,  $am_\infty = 0.2828$ ,  $\sigma = 3.46$ ; (c)  $64^3$ ,  $am_\infty = 0.1414$ ,  $\sigma = 0.1$ . For the SU(5)/SU(2) slope ratio, the same parameters as for (b) have been used.

axial gauge by minimizing unphysical high-momentum noise within 3-dimensional time slices. This turns out to be essential for our results for the spectra which would otherwise show much more power in the ultraviolet. Stable plasma modes are expected to contribute equally to  $f_A$  and  $f_E$ , whereas unstable modes are predominantly magnetic, leading to  $f_A > f_E$  in the corresponding momentum range.

Figure 6 shows the corresponding spectra, normalized per gluonic degree of freedom. The results are averaged over lattice vectors  $\mathbf{k}$  in 12 equally sized bins on a logarithmic scale along  $|\mathbf{k}^2|$ . In addition, SU(2) curves represent averages over 6 runs, while SU(3) curves represent averages over 4 runs.

The upper panel of Fig. 6 compares the magnetic ( $f_A(k)$ ) and electric ( $f_E(k)$ ) distribution functions. The lowest curves correspond to the initial time. Around  $k/m_\infty \sim 0.9$  there is a conspicuous exponential growth of modes associated with Weibel instabilities. In order to ease the comparison of  $f_A$  and  $f_E$  results, the time  $m_\infty \Delta t \approx 14$  is singled out in this plot by thick lines. As can be seen also in Fig. 1, the magnetic contributions dominate over electric contributions during the exponential growth phase. When non-Abelian self-interaction of the gluonic fields sets in, the exponential growth ceases, and only the higher modes  $k/m_\infty \gtrsim 2$  continue to grow, albeit more slowly.

A comparison between SU(2) and SU(3) is shown in the lower panel of Fig. 6. As expected, the behavior of the exponentially growing modes agrees well between the SU(2) and SU(3) calculations since in that regime non-Abelian self interactions are for the most part small. Note that the definitions (12) for  $f_A(k)$  and  $f_E(k)$  include a scaling by the number of degrees of freedom, which is proportional to  $N_g$ . This plot therefore corresponds to

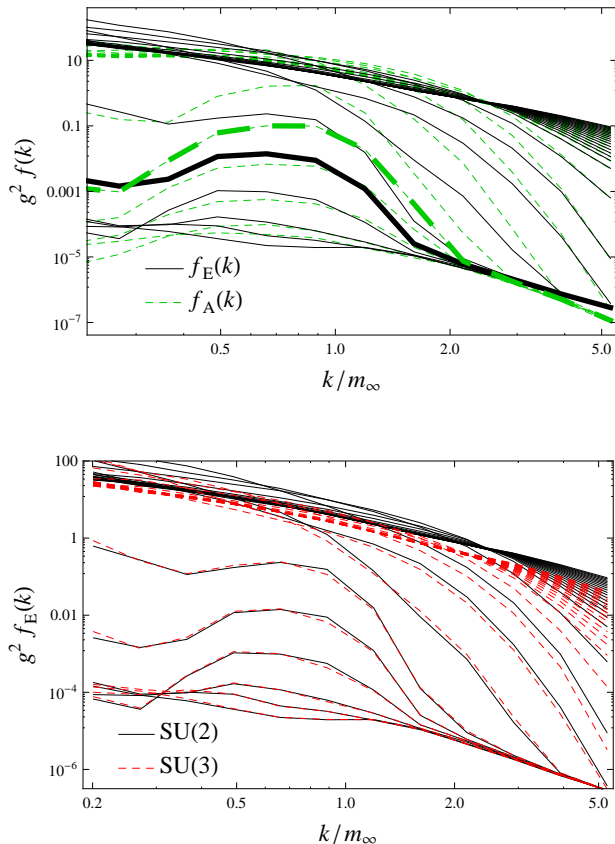


FIG. 6: (Color online.) Spectra corresponding to Fig. 1 for times  $0 \leq m_\infty t \lesssim 150$ . The distance between the lines is  $m_\infty \Delta t \approx 6$ . The upper panel shows the SU(2) spectra for the magnetic ( $f_A(k)$ ) and electric ( $f_E(k)$ ) distribution functions. The curves at time  $m_\infty t \approx 23$  are plotted with thick lines. The lower panel shows the electric ( $f_E(k)$ ) distribution functions for SU(2) vs. SU(3).

the energy density divided by  $N_g$  as depicted in Fig. 2. The evolution of the SU(2) and SU(3) curves only deviate from each other when non-linearities set in.

In order to study the non-Abelian regime with approximately linear growth of energies more carefully, Fig. 7 depicts the spectra multiplied by  $k^2$  and at late-time times  $80 \lesssim m_\infty t \lesssim 150$ . The distribution functions have been averaged over 32 bins along  $|\mathbf{k}^2|$  in these plots so that the large  $k$  region is better resolved. The slow growth at large momenta  $k/m_\infty \gtrsim 2$  corresponds to the linear growth regime of Fig. 1. On larger scales  $k/m_\infty \gtrsim 2$  we have  $f_A(k) \simeq f_E(k)$  as expected from stable modes in the perturbative regime. In an intermediate range  $0.5 \lesssim k/m_\infty \lesssim 2$ , magnetic fields dominate over electric ones  $f_A(k) > f_E(k)$ , which is caused by the predominantly magnetic plasma instabilities.

The straight lines in the upper panel of Fig. 7 correspond to simple power laws  $f(k) \sim k^{-\nu}$  with  $\nu = 2$

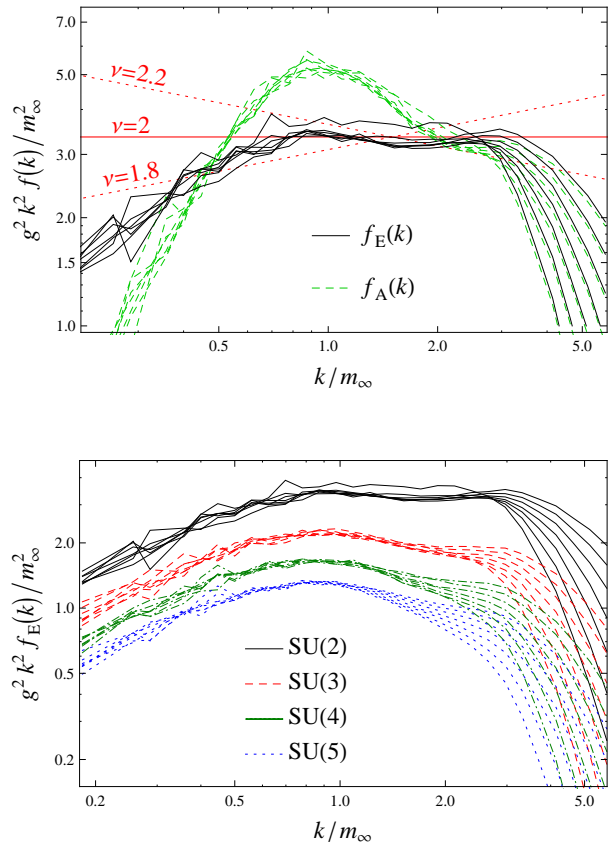


FIG. 7: (Color online.) The power spectrum for SU(2) of the Coulomb gauge distribution  $f(k)$  at late times  $80 \lesssim m_\infty t \lesssim 150$ . The distance between the lines is  $m_\infty \Delta t \approx 11$ . The upper panel shows a comparison for SU(2) for  $f_E(k)$  and  $f_A(k)$ . The straight central horizontal red line indicates a power law spectrum  $f \sim k^{-\nu}$  with  $\nu = 2$ , while the dotted lines correspond to  $\nu = 1.8$  and  $2.2$ . The lower panel compares the spectra  $f_E(k)$  for SU(2), SU(3), SU(4), and SU(5).

(straight line) and  $\nu = 1.8$ , and  $2.2$  (dotted lines). A distinct power law behavior  $\sim k^{-\nu}$  with  $\nu \approx 2$  over a large range of momenta can be most clearly extracted from the electric distribution function  $f_E(k)$ , which does not show a hump caused by the unstable magnetic modes, and if one excludes the higher momentum modes close to the lattice cutoff and also the largest times, where effects from the lattice cutoff may be felt. As error bar for  $\nu \approx 2$  we infer  $1.8 \lesssim \nu \lesssim 2.4$ .

The lower panel of Fig. 7 compares the electric field spectra  $f_E(k)$  at various gauge groups SU(2) through SU(5). The spectra of the various gauge groups appear to be similar, apart from an overall scaling factor.

#### IV. CONCLUSIONS

We have studied for the first time 3+1 dimensional simulations of non-Abelian plasma instabilities in the hard-loop framework for the gauge group SU(3) that is physically relevant for the physics of heavy-ion collisions. In order to study the dependence on the number of colors, we have also considered gauge groups SU(4) and SU(5). We have found that small seed fields which correspond to the same amount of initial energy density per gluon degree of freedom lead to comparable total energy density when exponential growth of plasma instabilities is stopped by nonabelian self-interactions and a phase of approximately linear growth begins. We have confirmed that in all nonabelian gauge groups considered a power-law spectrum  $f(k) \sim k^{-\nu}$  with  $\nu \approx 2$  develops for the higher-momentum modes, corresponding to a cascade of energy towards the ultraviolet. The growth rate of en-

ergy densities in this phase was found to scale roughly proportional to the number of colors.

#### Acknowledgments

This work has been supported by the Austrian Science Foundation FWF, project no. P19526. We would like to thank Paul Romatschke for communications and collaboration on the SU(2) code that was adapted for this work, and Maximilian Attems for assistance. We also gratefully acknowledge valuable discussions with Peter Arnold, Jürgen Berges, Dietrich Bödeker, Guy Moore, Al Mueller, Kari Rummukainen, and Larry Yaffe. The numerical calculations have been performed on the ECT\* Teraflop cluster, at the MPI Heidelberg parallel cluster, and at the Vienna Scientific Cluster.

- 
- [1] U. W. Heinz, AIP Conf. Proc. **739**, 163 (2005).
  - [2] E. S. Weibel, Phys. Rev. Lett. **2**, 83 (1959).
  - [3] P. Romatschke and M. Strickland, Phys. Rev. **D68**, 036004 (2003).
  - [4] P. Romatschke and M. Strickland, Phys. Rev. **D70**, 116006 (2004).
  - [5] F. Califano, N. Attico, F. Pegoraro, G. Bertin, and S. V. Bulanov, Phys. Rev. Lett. **86**, 5293 (2001).
  - [6] S. Mrowczynski, Phys. Lett. **B214**, 587 (1988).
  - [7] S. Mrowczynski, Phys. Lett. **B314**, 118 (1993).
  - [8] S. Mrowczynski and M. H. Thoma, Phys. Rev. **D62**, 036011 (2000).
  - [9] J. Randrup and S. Mrowczynski, Phys. Rev. **C68**, 034909 (2003).
  - [10] Y. E. Pokrovsky and A. V. Selikhov, JETP Lett. **47**, 12 (1988).
  - [11] Y. E. Pokrovsky and A. V. Selikhov, Sov. J. Nucl. Phys. **52**, 146 (1990).
  - [12] Y. E. Pokrovsky and A. V. Selikhov, Sov. J. Nucl. Phys. **52**, 385 (1990).
  - [13] O. P. Pavlenko, Sov. J. Nucl. Phys. **55**, 1243 (1992).
  - [14] S. Mrowczynski, Phys. Rev. **C49**, 2191 (1994).
  - [15] S. Mrowczynski, Phys. Lett. **B393**, 26 (1997).
  - [16] P. Arnold, J. Lenaghan, and G. D. Moore, JHEP **08**, 002 (2003).
  - [17] P. Arnold, J. Lenaghan, G. D. Moore, and L. G. Yaffe, Phys. Rev. Lett. **94**, 072302 (2005).
  - [18] A. Rebhan, P. Romatschke, and M. Strickland, Phys. Rev. Lett. **94**, 102303 (2005).
  - [19] P. Arnold, G. D. Moore, and L. G. Yaffe, Phys. Rev. **D72**, 054003 (2005).
  - [20] A. Rebhan, P. Romatschke, and M. Strickland, JHEP **09**, 041 (2005).
  - [21] A. Dumitru, Y. Nara, B. Schenke, and M. Strickland, Phys. Rev. **C78**, 024909 (2008).
  - [22] A. Dumitru, Y. Nara, and M. Strickland, Phys. Rev. **D75**, 025016 (2007).
  - [23] A. Dumitru and Y. Nara, Phys. Lett. **B621**, 89 (2005).
  - [24] P. Romatschke and R. Venugopalan, Phys. Rev. Lett. **96**, 062302 (2006).
  - [25] P. Romatschke and R. Venugopalan, Phys. Rev. **D74**, 045011 (2006).
  - [26] P. Romatschke and A. Rebhan, Phys. Rev. Lett. **97**, 252301 (2006).
  - [27] A. Rebhan, M. Strickland, and M. Attems, Phys. Rev. **D78**, 045023 (2008).
  - [28] A. Rebhan and D. Steineder, Phys. Rev. **D81**, 085044 (2010).
  - [29] D. Bödeker and K. Rummukainen, JHEP **07**, 022 (2007).
  - [30] P. Arnold and G. D. Moore, Phys. Rev. **D76**, 045009 (2007).
  - [31] P. B. Arnold and G. D. Moore, Phys. Rev. **D73**, 025006 (2006).
  - [32] J. Berges, S. Scheffler, and D. Sexty, Phys. Rev. **D77**, 034504 (2008).
  - [33] J. Berges, S. Scheffler, and D. Sexty, Phys. Lett. **B681**, 362 (2009).
  - [34] P. B. Arnold and G. D. Moore, Phys. Rev. **D73**, 025013 (2006).
  - [35] A. H. Mueller, private communication.
  - [36] D. Bödeker, JHEP **10**, 092 (2005).
  - [37] A. H. Mueller, A. I. Shoshi, and S. M. H. Wong, Phys. Lett. **B632**, 257 (2006).
  - [38] A. H. Mueller, A. I. Shoshi, and S. M. H. Wong, Eur. Phys. J. **A29**, 49 (2006).
  - [39] M. Asakawa, S. A. Bass, and B. Muller, Phys. Rev. Lett. **96**, 252301 (2006).
  - [40] A. H. Mueller, A. I. Shoshi, and S. M. H. Wong, Nucl. Phys. **B760**, 145 (2007).
  - [41] A. Majumder, B. Muller, and S. A. Bass, Phys. Rev. Lett. **99**, 042301 (2007).
  - [42] M. E. Carrington and A. Rebhan, arXiv:1011.0393, 2010.
  - [43] J. Berges, D. Gelfand, S. Scheffler, and D. Sexty, Phys. Lett. **B677**, 210 (2009).
  - [44] J.-P. Blaizot and E. Iancu, Phys. Rept. **359**, 355 (2002).
  - [45] R. D. Pisarski, hep-ph/9710370, 1997.
  - [46] S. Mrowczynski, A. Rebhan, and M. Strickland, Phys. Rev. **D70**, 025004 (2004).

- [47] J. P. Blaizot and E. Iancu, Nucl. Phys. **B417**, 608 (1994).
- [48] G. D. Moore and N. Turok, Phys.Rev. **D56**, 6533 (1997).